Advances in Aircraft and Spacecraft Science, *Vol. 6, No. 3 (2019) 225-238*
DOI: https://doi.org/10.12989/aas.2019.6.3.225

Measured aerodynamic coefficients of without and with spiked blunt body at Mach 6

R. Kalimuthu[1a], R. C. Mehta*[2] and E. Rathakrishnan[3c]

[1]*Vikram Saarabhai Space Centre, Trivandrum 695022, India*
[2]*Department of Aeronautical Engineering, Noorul Islam Centre for Higher Education, Kumaracoil 629180, India*
[3]*Department of Aerospace Engineering, Indian Institute of Technology, Kanpur 208016, India*

(Received August 20, 2018, Revised December 31, 2018, Accepted January 10, 2019)

Abstract. A spike attached to a blunt nosed body significantly alters its flow field and influences the aerodynamic coefficients at hypersonic speed. The basic body is an axisymmetric, with a hemisphere nose followed by a cylindrical portion. Five different types of spikes, namely, conical aerospike, hemisphere aerospike, flat-face aerospike, hemisphere aerodisk and flat-face aerodisk are attached to the basic body in order to assess the aerodynamic characteristic. The spiked blunt body without the aerospike or aerodisk has been set to be a basic model. The coefficients of drag, lift and pitching moment were measured with and without blunt spike body for the length-to-diameter ratio (L/D) of 0.5, 1.0, 1.5 and 2.0, at Mach 6 and angle of attack up to 8 degrees using a strain gauge balance. The measured forces and moment data are employed to determine the relative performance of the aerodynamic with respect to the basic model. A maximum of 77 percent drag reduction was achieved with hemisphere aerospike of L/D = 2.0. The comparison of aerodynamic coefficients between the basic model and the spiked blunt body reveals that the aerodynamic drag and pitching moment coefficients decrease with increasing the L/D ratio and angle of attack but the lift coefficient has increasing characteristics.

Keywords: aerodynamics coefficients; aerospike; aerodisk; blunt body; fluid dynamics; hypersonic flow; pitching moment; shock wave; space vehicle

1. Introduction

Experimental Investigation on the influence of the spike on the aerodynamic characteristics of blunt bodies has attracted interest of many researchers for a long time. Early experimental investigations were done using thin protruding probe placed in front of blunt bodies at supersonic and hypersonic speeds. A study on bodies of revolution with flat and hemispherical nose shapes and with and without thin protruded probes of different length was carried out (Mair 1952) for Mach 1.96. The physical process of the change of shock wave shape over the spiked body has been described by (Moeckel 1951). The flow characteristics can be changed by varying the length and diameter of a probe. Jones (1952) measured drag with a balance for different bluntness ratio bodies

*Corresponding author, Professor, E-mail: drrakhab.mehta@gmail.com
[a]Ph.D., E-mail: rkpearlsa@gmail.com
[b]Professor, E-mail: erath@iitk.ac.in

http://www.techno-press.org/?journal=aas&subpage=7 ISSN: 2287-528X (Print), 2287-5271 (Online)

at $M_\infty = 2.72$ and Reynolds number 1.83 x 10^6 at zero-degree angle of incidence. He found that the drag is increasing with the bluntness of the body and it is a minimum value if the nose radius is more than 0.25 of radius of blunt body. Daniel and Yoshihara (1993) experimentally compared the drag force on the sharp cone tipped spike (semi-cone angle 10 degree) to that flat-nosed tip with equal diameter of the spike at zero angle of attack. They found that C_D is larger with a spike cone-tip, compared with a blunt nose spike at all lengths of the spike. It was observed that at Mach = 2.5 with $L/D = 2.4$ for the spike, C_D is reduced from 0.29 to 0.283, if the spike is flat. At $L/D = 3.0$, C_D is reduced from 0.394 to 0.342. Maull (1960) did experiments on spiked blunt body, in the Imperial college hypersonic gun tunnel at Mach 6.8. Wood (1961) carried out experiments on spike body with cone cylinder at Mach 10. They observed from these experiments that the reattachment point remains close to the shoulder of the body. A summary of experimental investigations up to 1966 has been reported by Chang (1970) for axially symmetric model with various spikes shape in the freestream Mach number range of $1.75 \leq M_\infty \leq 14$ and Reynolds number range (based upon the blunt after bodies diameter) range of $0.85 \times 10^6 \leq Re \leq 1.5 \times 10^6$.

Motoyama *et al.* (2001) experimentally investigated the drag reduction on hemispherical body using different spike with two different lengths-to-diameter ratios at Mach 7. Menezes *et al.* (2002a) did work on shock tunnel study of spiked aerodynamic bodies flying at hypersonic Mach 5.75. Experiments on large blunt-nosed cone with spike attachments were carried out by Menezes *et al.* (2002b). Ahmed and Qin (2011) provided a detailed review on the spiked hypersonic vehicle, and they also pointed out that some areas in this field need further investigation. Wang *et al.* (2016) have reviewed experimental data at hypersonic speeds.

Yadav and Guven (2013) developed the concept of double-disk aerospikes, which favourably reduced turbulent reattachment heat flux and drag on the main body. The flow fields over a blunt cone with and without aerodisk at hypersonic speeds are investigated by Huang *et al.* (2017). Gerdroodbary *et al.* (2010) have investigated effectiveness of aerodisk/aerospike assemblies as retractable drag reduction devices for large angle blunt cones operated at Mach 5.75. Deng *et al.* (2017) have investigated the pressure distribution and aerodynamic drag characteristics by simulating and comparing the lifting body with or without the aerospike at Mach 8. Sebastian *et al.* (2016) have numerically analyzed performance at Mach 6 and different length-to-diameter ratio at different angle of attack. Schülein (2008) proposed a pivoting self-aligning spike to improve aerodynamic effectiveness at a wide range of angles of attack.

From the above literature survey, it is evident that, even though spikes for drag reduction at hypersonic Mach numbers have been investigated extensively, almost all of them focus only on limited parameters, such as a particular spike shape, and spike length.

The features of the high-speed flowfield can be delineated through these experimental (Kalimuthu *et al.* 2008a, 2017b) and numerical (Mehta 2010a, b) and (Yamauchi *et al.* 1993) studies. Based on these investigations a schematic of the flowfield around the blunt-body, the conical, the hemispherical and the flat-face spiked blunt body at zero angle-of incidence is delineated in Fig. 1. A blunt nose in supersonic flight is accompanied by a bow shock wave. A hemi-spherical portion of the blunt body is accomplished by a bow shock wave as depicted in Fig. 1(a). A well-known concept for reducing the impact of the bow shock wave on a blunt body, while keeping a blunt nose, is the aerospike. The simplest aerospike design is a conical aerospike mounted on the tip of a blunt body as depicted in Fig. 1(b). For the aerospike in ideal case, the boundary layer separates along the whole spike surface due to the pressure rise over the bow shock wave. The separated boundary layer forms a shear layer that reattached on the blunt nose. Due to the shear layer, the outer supersonic bow is detected and a weaker conical shock is

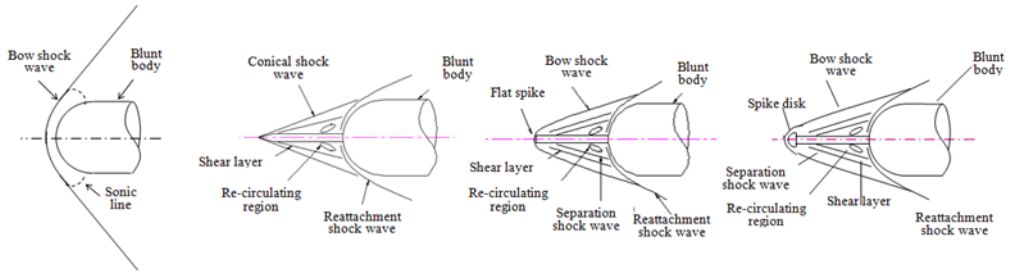

Fig. 1 Flow field features around without and with spiked blunt bodies at high-speeds (a) basic body, (b) conical spike, (c) Flat-face spike and (d) hemisphere aerodisk

formed instead of the initial bow shock. The conical shock unites with the reattachment shock further downstream. A recirculation zone forms inside the shear surface and shows significantly lower pressure levels compared with the blunt body without an aerospike. In the case of the flat-face and the hemispherical aerospikes observe a formation of a bow shock wave ahead of the body as delineated in Fig. 1(c) and 1(d). The flow separation zone is noticed around the root of the spike up to the reattachment point of the flow at the corner of the blunt body. Due to the recirculating region, the pressure at the stagnation region of the blunt body will reduce. However, because of the reattachment of the shear layer on the corner of the blunt-body, the pressure near the reattachment point becomes large. Whether the reattachment point can be depends on the geometrical parameters of the spike or the blunt body configuration. The spike is characterized by a free shear layer, which is formed as a result of the flow separating from spike leading edge and reattaching to the blunt body, essentially bridging the spike. The separating shear layer from the spike leading edge of the aerospike attaches to the blunt body after entering through an expansion fan at the leading edge corner and a recompression shock at attachment point. The attached shear layer then separates near the trailing edge and generates a separation shock before reattaching point at the trailing edge prior to undergoing flow expansion. The separated boundary layer forms a shear layer that reattaches on the blunt nose.

The main aim of the present paper to assess the performance of aerodynamic coefficients without and with aerospike and aerodisk attached to a blunted body. The drag and normal force acting on the basic body with and without spike were measured directly with internal balance data in order to understand the behavior of the aerodynamic coefficients for L/D ratio of 0.5, 1.0, 1.5 and 2.0 at Mach 6 and at angle of attack α varies from 0 to 8 degrees. It is important to mention here that the comparative analysis of the aerodynamic coefficients between the basic model and with aerospike and aerodisk attached to the blunted body was not carried out earlier.

2. Test facilities

2.1 Hypersonic wind-tunnel

The hypersonic wind tunnel used for this study is an axisymmetric, enclosed free-jet wind tunnel with a free-jet diameter of 25.0×10^{-2} m. The tunnel system is having high pressure air supply, a pebble bed heater, contoured nozzles for delivering flow of the required Mach number, a free jet test-section, a fixed geometry diffuser with scoop to collect the nozzle flow and the

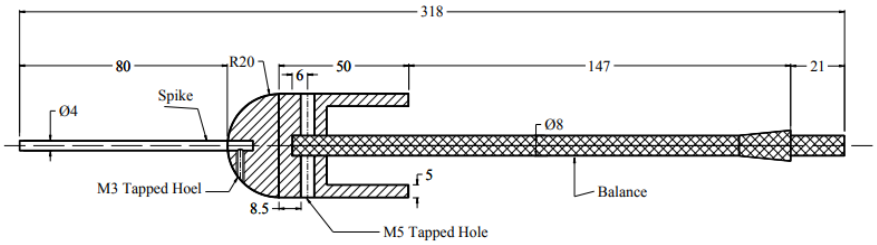

Fig. 2 Strain gauge balance attachment

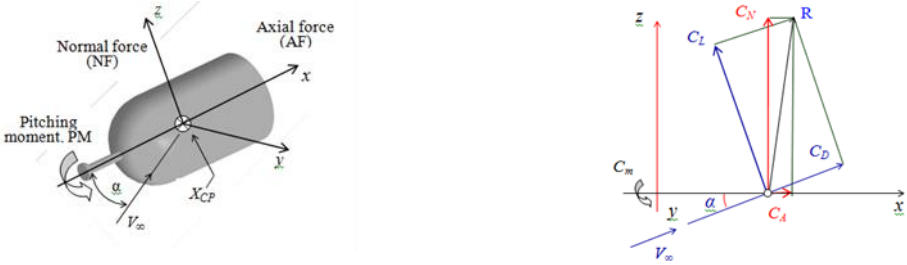

(a) (b)

Fig. 3 Sign convention used for forces measurement studies

vacuum system. A stainless-steel contoured nozzle of fixed exit diameter of 25.4×10^{-2} m is used to obtain Mach 6 in the test section. The Reynolds number is 18×10^6 based on the free-jet diameter. The maximum running time of wind tunnel is 35s.

2.2 Force measurements

Angle of attack was covered in these experiments 0 to 8 degrees using pitching mechanism. A six-component integral type strain gauge balance diameter of 8.0×10^{-3} m is used for force measurements. The strain gauge balance is capable of measuring normal and axial force and pitching moment. The balance is calibrated before doing the tests. Ensuring the check load with actual load applied, the balance is used for the tests. After mounting the model with balance in the test-section, the weight of the model was measured using the calibration matrix through data acquisition mode. It was measured within ±1% of actual load, using a normal digital weigh balance. Fig. 2 shows the strain gauge balance attachment. The angle of attack was covered from 0–8 degrees in interval of 0.133 degree. Detail of the hypersonic wind tunnel and the strain gauge are described in detail (Kalimuthu 2009).

2.3 Data acquisition and processing

Force measurement data acquisition and processing is essentially carried out by a DAC in the computer. The computer software can control the functions of the DAC and the acquired data is transferred to the computer during the test through a signal conditioner, amplifier and ADC card. A manual trigger signal from the tunnel control console initiates the data acquisition. This trigger signal also initiates the computer to acquire the data from the total pressure transducer, pitot pressure transducer, the angle of attack signal from the potentiometer of the pitching mechanism

and force measurements data. Data acquisition is terminated when the pitching mechanism reached angle of attack 8 degree. The analogue signal is digitized by an ADC card in the computer. Data acquired by the ADC in the computer are subsequently processed by separately to get all aerodynamic coefficients.

The normal force (*NF*) and the axial force (*AF*) component as depicted in Fig. 3 (a) were measured by Kalimuth*et al.* (2008a and 2017b). Fig. 3 depicts sign convention used for forces measurement studies. Body axis aerodynamics coefficient (Fig. 3(b)) like C_N and C_A is converted to wind axis aerodynamic coefficients of C_L and C_D. The wind axis aerodynamics relation is given below

$$\begin{aligned} C_A &= \frac{AF}{q_\infty S} \\ C_N &= \frac{NF}{q_\infty S} \\ C_L &= C_A * cos\,\alpha + C_N * sin\,\alpha \\ C_D &= C_N * cos\,\alpha - C_A * sin\,\alpha \\ C_{PM} &= \frac{PM}{q_\infty SL} \end{aligned} \tag{1}$$

where *AF*, *NF* and *PM* are the axial force, normal force and pitching moment respectively. *L* is the length of the spike, α is the angle of attack, q_∞ is the freestream dynamic pressure and *S* is the reference area based on the cylinder diameter *D*.

3. Experimental models

3.1 Basic model

The basic configuration consisted of hemisphere 4 $\times 10^{-2}$ m diameter followed by a 5 $\times 10^{-2}$ m length of cylinder. Two basic models were designed and fabricated. One model consisted of hemisphere with cylinder and 4 $\times 10^{-3}$ m diameter of hole at a stagnation point for fixing the spike. Spike was attached with the parental body using a M3 screw. Second model of basic configuration was without hole at the stagnation point location. Details of the basic configuration are shown in Fig. 4(a).

3.2 Spiked model

Basic configuration showing the attachment details for spike is shown schematically in Figs. 4(b) and 4(c). Configurations studied in the present investigation are conical aerospike, flat-face aerospike, hemisphere aerospike, hemisphere aerodisk, and flat face aerodisk.

The conical aerospike studied was of diameter 4.0 $\times 10^{-3}$ m and semi-cone angle 15 degree. Flat-face aerospike was of circular rod 4.0 $\times 10^{-3}$ m diameter with a flat-face. The hemisphere aerospike has a diameter of 4.0 $\times$ 10^{-3} m and hemisphere of nose of 2.0 $\times$ 10^{-3} m radius. The hemisphere aerodisk has a diameter of 4.0 $\times$ 10^{-3} m and cap shaped nose of 4.0 $\times$ 10^{-3} m radius.

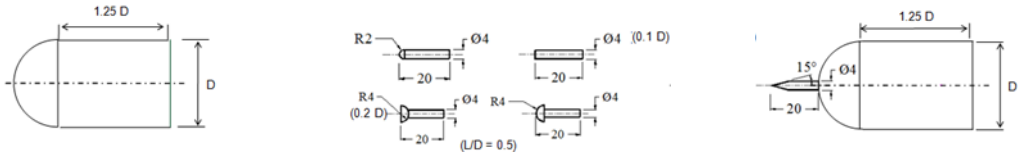

(a) (b) (c)

Fig. 4 Geometrical details of (a) basic model, (b) spikes and (c) spiked blunt body

The flat-face aerodisk has a diameter of 4.0×10^{-3} m and 4.0×10^{-3} m radius cap fixed in inverted position. The geometrical details of these spikes are shown in Fig. 4 (b).

Four spikes of length L 2.0×10^{-2} m, 4.0×10^{-2} m, 6.0×10^{-2} m and 8.0×10^{-2} m were designed and fabricated for the configurations considered. The length L of these spikes was non-dimensionlized with the cylinder diameter, D. Spikes of L/D = 0.5, 1.0, 1.5 and 2.0 were studied for all the configurations.

4. Results and discussion

A forward-facing spike attached to a hemisphere body (basic body) alters the flow field around and influence the aerodynamic forces at hypersonic speed.

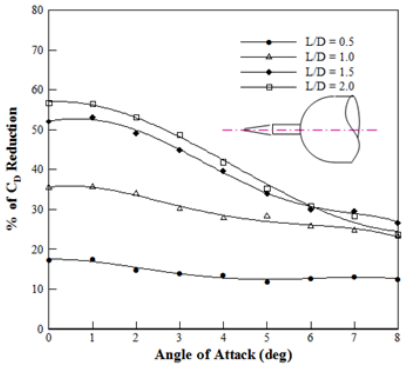

Fig. 5 Percentage of C_D reduction for different L/D of conical aerospike

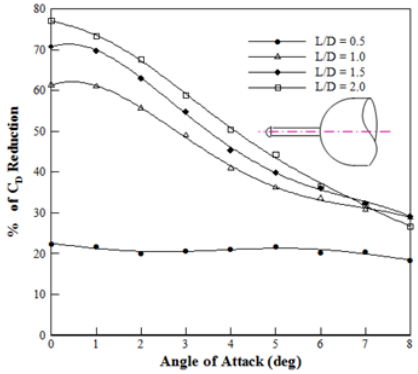

Fig. 6 Percentage of C_D reduction for different L/D of hemisphere aerospike

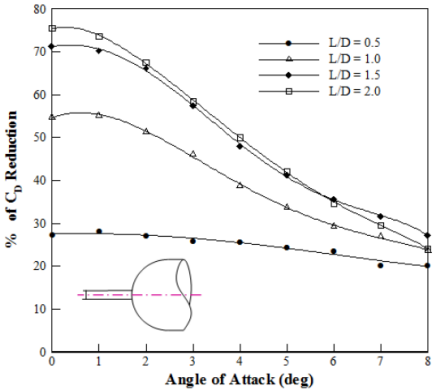

Fig. 7 Percentage of C_D reduction for different *L*/*D* of flat-face aerospike

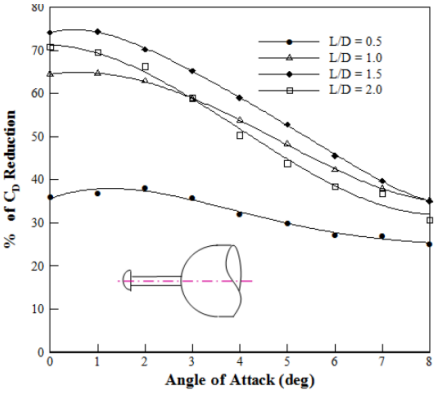

Fig. 8 Percentage of C_D reduction for different *L*/*D* of hemisphere aerodisk

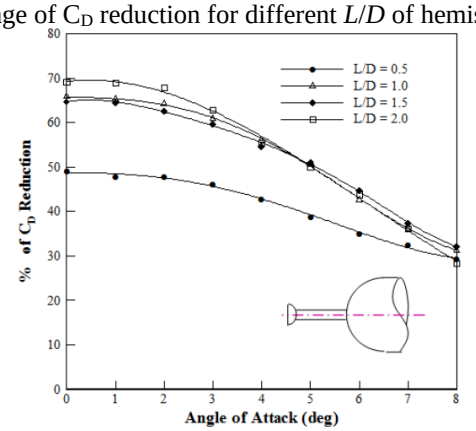

Fig. 9 Percentage of C_D reduction for different *L*/*D* of flat-face aerodisk

From sting balanced measurements, aerodynamic coefficients drag, lift and pitching moment on the body without spike and with conical aerospike, flat-face aerospike, hemisphere aerospike, flat-face aerodisk of length-to-diameter ratio, *L*/*D* = 0.5, 1.0, 1.5 and 2.0, at angle of attack 0 to 8 degrees are calculated employing Eq. (1).

4.1 Aerodynamic coefficients with respect to basic body

4.1.1 Aerodynamic drag coefficient

It is found that the drag coefficient is nearly independent of angle of attack in the case of basic model as measured in Kalimuthu (2009). Fig. 5 shows the percentage C_D reduction for the conical aerospike at different L/D ratio and angles of attack. It is seen from the measured data for angle of attack 0 to 6 degrees that the maximum reduction is achieved for L/D = 2.0. A maximum of about 55% reduction in the drag coefficient is achieved for spike of L/D = 2.0 in the range of angle of attack from 0 to 2 degrees.

The percentage reduction of C_D for the hemisphere aerospike is shown in Fig. 6. For the hemisphere aerospike the maximum C_D reduction is about 77% at zero angle of attack. The non-linearity of these curves increases marginally compared to the conical aerospike. For the hemisphere aerospike case also, for angle of attack from 0 to 6 degrees, L/D = 2 results in maximum reduction of C_D. It also shows in the minimum reduction of C_D at L/D = 0.5

The percentage reduction of C_D for the flat-face aerospike is shown in Fig. 7. It is observed that, the performance of L/D = 1.5 and 2.0 are closer at angles of attack 2 degrees and above. The C_D levels for the flat-face aerospike is almost the same as that of the hemisphere aerospike at all angles of attack.

The percentage variation of C_D with different L/D ratio and angle of attack is depicted in Fig. 8 for the hemisphere aerodisk. The maximum reduction of C_D is found for L/D = 1.5, unlike the other cases where the maximum reduction of C_D is noticed at L/D = 2.0.

The percentage of C_D reduction for the flat-face aerodisk is shown in Fig. 9. The performance of L/D = 1.0, 1.5 and 2.0 are close to each other as can be seen in Fig. 9. A continuous decreasing trend of percentage reduction in C_D is observed. The maximum decrease in C_D is occurred at L/D = 2.0 and $\alpha = 0 - 3$ degrees.

4.1.2 Normal force coefficient

When a spiked is attached to the blunt body (basic body), at an angle of attack, there will be a normal force due to the spike (referred to as lift in the present analysis). At many situations, this is an undesirable force which has to be balanced by some control devices.

Fig. 10 depicts the variation of ΔC_L versus α for the conical spike for different L/D. For the spike of L/D = 0.5, the variation of C_L shows similar trend in the case of the basic body. The magnitude of C_L is significantly higher than the basic body at all angles of attack as mentioned in Kalimuthu (2009). The ΔC_L differences monotonically increase with increase of angle of attack. For L/D = 1.0, 1.5 and 2.0 the variation of ΔC_L with angle of attack becomes non-linear. The ΔC_L becomes independent of angle of attack for more than 5 degree and for L/D = 1.5 and 2.0. As seen earlier, the best reduction in ΔC_L is found at L/D = 0.5 at all angles of attack. As expected, the maximum ΔC_L is for L/D = 2, at all angle of attacks and the minimum ΔC_L is for L/D = 0.5.

The variation of ΔC_L increases with α for the hemisphere aerospike as shown in Fig. 11. It can also observe from the figure that the ΔC_L increase is largest for L/D = 2.0 at all angles of attack.

The increase of ΔC_L for the flat-face aerospike is shown in Fig. 12. For the flat-face aerospike also, the maximum increase in ΔC_L for L/D = 2.0 and the minimum is for L/D = 0.5.

The ΔC_L is having increasing variation with α for the hemisphere aerodisk (Fig. 13). The maximum increase in ΔC_L is occurred for L/D = 2.0, for angle of attack 0 to 6 degrees. For $\alpha > 6$ degree, the increasing trend in ΔC_L for 1.5 and 2.0 is almost identical.

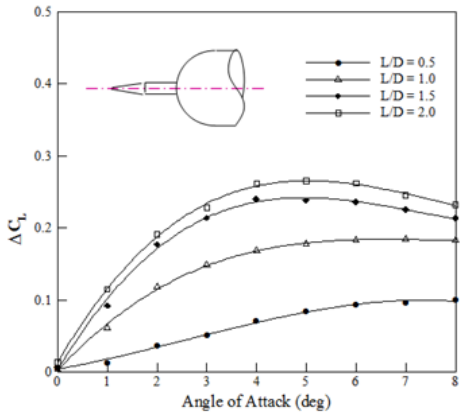

Fig. 10 ΔC_L increase for different L/D of conical aerospike

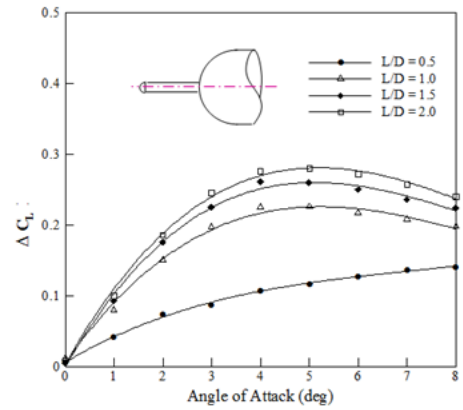

Fig. 11 ΔC_L increase for different L/D of hemisphere aerospike

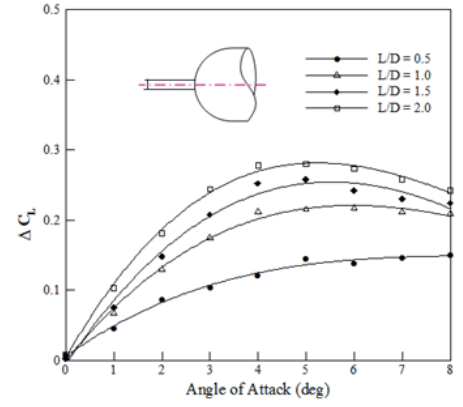

Fig. 12 ΔC_L increase for different L/D of flat-face aerospike

The ΔC_L is also having continuous increasing trend for L/D = 1.0, 1.5 and 2.0 for the flat-face aerodisk. However, they are close to each other as can be visualized in Fig. 14.

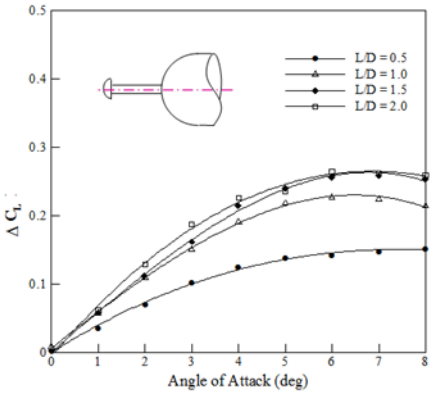

Fig. 13 ΔC_L increase for different *L*/*D* of hemisphere aerodisk

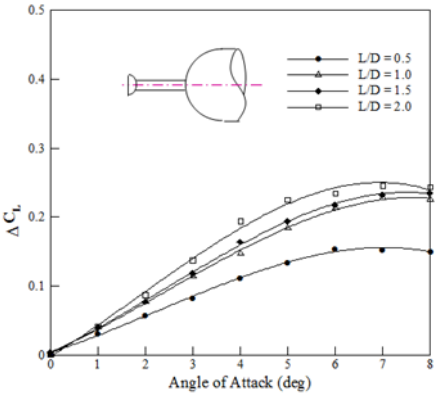

Fig. 14 ΔC_L increase for different *L*/*D* of flat-face aerodisk

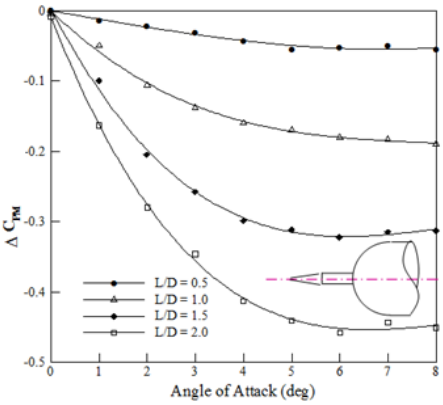

Fig. 15 ΔC_L increase for different *L*/*D* of flat-face aerodisk

4.1.3 Pitching moment coefficient

For the basic body, the pitching moment is about the nose of the body. As typical of the body under consideration the pitching moment of the basic body decreases with increasing of angle of

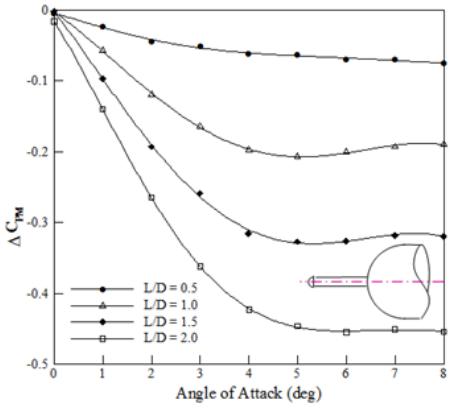

Fig. 16 ΔC_{PM} increase for different L/D of hemisphere aerospike

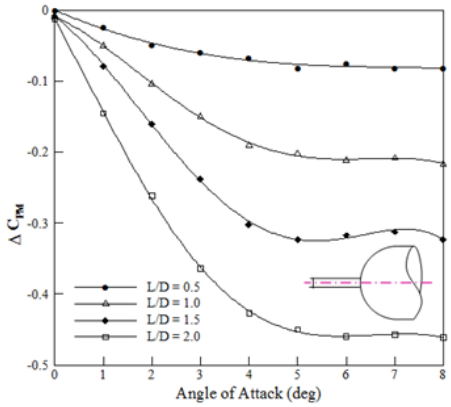

Fig. 17 ΔC_{PM} increase for different *L*/*D* of flat-face aerospike

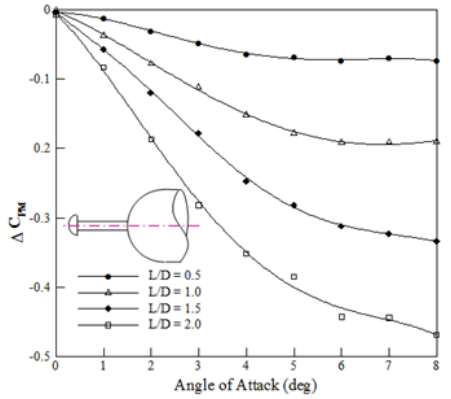

Fig. 18 ΔC_{PM} increase for different *L*/*D* of hemisphere aerodisk

attack as can be seen in the measured data of Kalimuthu (2009). In the present analysis, the nose up moment is taken as positive and nose down moment is taken as negative. As in the case of basic body, for *L*/*D* = 0.5 also the pitching moment decreases with increase of angle of attack, almost

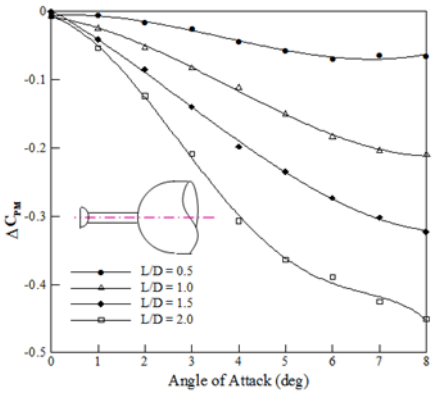

Fig. 19 ΔC_{PM} increase for different L/D of flat-face aerodisk

linearly at all levels of angle of attack. The variation of C_{PM} with angle of attack becomes non-linear. Also, the rate of decrease of C_{PM} with increase of angle of attack becomes faster with increase of L/D. The pitching moment is based on the moment about the center of gravity. Therefore, the center of pressure X_{CP} assumes positions upstream of the basic body nose. It is important to mention here that consideration for compensation of the increase pitching moment is required in order to account the usefulness of the spike in various angle of attack situations.

Fig. 15 shows the ΔC_{PM} increase with angle of attack, for the conical aerospike. The maximum C_{PM} (negative) is for $L/D = 2$ at all angles of attack, and the negative C_{PM} decreases with decrease in L/D at all angles of attack.

For the hemisphere aerospike the ΔC_{PM} increase shown in Fig. 16 reveals that the ΔC_{PM} decrease with increase of L/D up to about angle of attack 4 degrees and the variation of ΔC_{PM} with angle of attack is found marginal for $\alpha > 4$.

The ΔC_{PM} levels for the flat-face aerospike (Fig. 17) are almost the same as the conical aerospike at all angles of attack. For the flat face aerospike, also ΔC_{PM} decreases rapidly with angle of attack from 0 to 4 degrees and beyond that ΔC_{PM} decrease is observed marginal.

Fig. 18 shows the variation of ΔC_{PM} increase with angle of attack for the hemisphere aerodisk, it is interesting to see that, for $L/D = 2.0$ the ΔC_{PM} decreases continuously with angle of attack. But for decreasing L/D, the decrease of ΔC_{PM} is steep up to angle of attack 5 degrees and beyond that the rate of decrease comes down.

As in the case of the hemisphere aerodisk, for flat face aerodisk also ΔC_{PM} (Fig. 19) comes down continuously for $L/D = 2.0$ and 1.5, but for $L/D = 1.0$ and 0.5, the rate of decrease reduces with increase in angle of attack.

5. Conclusions

A spike attached to a hemisphere body drastically changes the flow field around the basic body and influences the aerodynamic drag at hypersonic flow. In other words, by fixing a spike, the detached shock at the nose of the basic body is essentially shifted to the nose of the spike, which is much smaller than the body nose. An experimental investigation was performed to measure aerodynamic forces for spikes attached to blunt bodies with conical, hemispherical and flat-face spike at Mach 6 and at an angle of attack range from 0 to 8 deg and length-to-diameter L/D ratio of

spike varies from 0.5 to 2.0. The measured data are analyzed to assess the relative performance of aerodynamic coefficient without and with spiked blunt body. The influence of geometrical parameters of the spike, the shape of the spike-tip and the angle-of-attack on the aerodynamic coefficients are investigated by measuring aerodynamic forces in a hypersonic wind tunnel.

It is found that a maximum reduction of drag of about 77% was found for hemisphere spike of L/D = 2.0 at zero angle of attack. Consideration for compensation of increased pitching moment is required to stabilize the aerodynamic forces. Among the spikes studied, the most efficient one is the hemispherical aerospike with L/D = 2.0. This causes a maximum drag reduction of about 77% at zero angle of attack. This spikes essentially shifts the strong detached shock at the nose of the basic body to the nose of the spike, also the detached shock is rendered weak because of the smaller radius of the spike nose. These changes cause a drastic reduction of aerodynamic drag.

The comparison between aerodynamic coefficients between the basic model and with the spike attached to the blunt body reveals that the drag and the pitching moment decreasing with the increase L/D ratio and angle of attack while the lift coefficient is having an increasing profile.

References

Ahmed, M.Y.M. and Qin, N. (2011), "Recent advances in the aerothermodynamics of spiked hypersonic vehicles", *Prog. Aerosp. Sci.*, **47**(6), 425-449. https://doi.org/10.1016/j.paerosci.2011.06.001.

Chang, P.L. (1970), *SEPRATION OF FLOW*, Pergamon Press, Oxford, U.K.

Daniels, L.E. and Yoshihara, H. (1954), "Effect of the upstream influences of a shock wave at supersonic speeds in the presence of a separated boundary flows", WADC Technical Report, U.S.A.

Deng, F., Liang, B., Xie, F. and Qin, N. (2017), "Spike effects on drag reduction for hypersonic lifting body", *J. Spacecraft Rockets*, **54**(6), 1185-1195. https://doi.org/10.2514/1.A33865.

Gerdroodbary, M.B. and Hosseinalipour, S.M. (2010), "Numerical simulation of hypersonic flow over highly blunted cones with spike", *Acta Astronautica*, **67**(1-2), 180-193. https://doi.org/10.1016/j.actaastro.2010.01.026.

Huang, W., Li, L., Yan, L.Q. and Zhang, T.T. (2017), "Drag and heat flux reduction mechanism of blunted cone and aerodisks", *Acta Astronautica*, **136**, 168-178. https://doi.org/10.1016/j.actaastro.2017.05.040.

Jones, J.J. (1952), "Flow separation from rods ahead of Blunt Nose at Mach number 2.72", *NACA RM, L52E05a*, U.S.A.

Kalimuthu, R. (2009), "Experimental investigation of hemispherical nosed cylinder with and without spike in a hypersonic flow", Ph. D. Thesis, Indian Institute of Technology, Kanpur, India.

Kalimuthu, R., Mehta, R.C. and Rathakrishnan, E. (2008a), "Experimental investigation on spiked body at hypersonic flow", *Aeronaut. J.*, **112**(1136), 593-598. https://doi.org/10.1017/S0001924000002554.

Kalimuthu, R., Mehta, R.C. and Rathakrishnan, E. (2017b), "Investigation of aerodynamic coefficients at Mach 6 over conical, hemispherical and flat-face spiked body", *Aeronaut. J.*, **121**(1245), 1711-1732. https://doi.org/10.1017/aer.2017.100.

Mair, W.A. (1952) "Experiments on separation of boundary layers on probes in front of blunt-nosed bodies in a supersonic air stream", *Phil. Mag. J. Sci.*, **43** (342), 695-716. https://doi.org/10.1080/14786440708520987.

Maull, D.J. (1960), "Hypersonic flow over axially symmetric spiked bodies", *J. Fluid Mech.*, **8**, 584-594. https://doi.org/10.1017/S0022112060000815.

Mehta, R.C. (2010a), "Numerical simulation of the flow field over conical, disk and flat spiked body at Mach 6", *Aeronaut. J.*, **114** (1154), 225-236. https://doi.org/10.1017/S0001924000003675.

Mehta, R.C. (2013b), "Numerical heat transfer study around a spiked blunt-nose body at Mach 6", *Heat Mass Transfer*, **49**(4), 485-496. https://doi.org/10.1007/s00231-012-1095-6.

Menezes, V., Saravanan, A. and Reddy, K.P.J. (2002a), "Shock tunnel study of spiked aerodynamic bodies

flying at hypersonic Mach number", *Shock Waves*, **12**, 197-204. https://doi.org/10.1007/s00193-002-0160-3.

Menezes, V., Saravanan, S., Jagadeesh, G. and Reddy, K.P.J. (2009b), "Aerodynamic drag reduction using aerospikes for large angle blunt cone flying at hypersonic Mach number", *Proceedings of the 22nd AIAA Aerodynamic Measurement Technology and Ground Testing Conference*, St. Louis, Missouri, U.S.A., June.

Moeckel, W.E. (1951), *Flow Separation Ahead of Blunt Bodies at Supersonic Speeds*, NACA TN-2418, U.S.A.

Motoyama, N., Mihara, K., Miyajima, R., Watanuki, T. and Kubota, H. (2001), "Thermal protection and drag reduction with use of spike in hypersonic flow", AIAA paper 2001-1828, U.S.A.

Schülein, E. (2008), "Wave drag reduction approach for blunt bodies at high angles of attack: proof-of-concept experiments", AIAA Paper 2008-4000, U.S.A.

Sebastian, J.J., Suryan, A. and Kim, H.D. (2016), "Numerical analysis of hypersonic flow past blunt bodies with aerospikes", *J. Spacecraft Rockets*, **53**(4), 669-677. https://doi.org/10.2514/1.A33414.

Wang, Z.G., Sun, X.W., Huang, W., Li, S.B. and Yan, L. (2016), "Experimental investigation on drag and heat flux reduction in supersonic/hypersonic flows: A survey", *Acta Astronautica*, **129**, 95-110. https://doi.org/10.1016/j.actaastro.2016.09.004.

Wood, C.J. (1961), "Hypersonic flow over spiked cones", *J. Fluid Mech*., **12**(4), 614-624. https://doi.org/10.1017/S0022112062000427.

Yadav, R. and Guven, U. (2013), "Aerothermodynamics of a hypersonic projectile with a double-disk aerospike", *Aeronaut. J*., **117**(1195), 913-928. https://doi.org/10.1017/S0001924000008587.

Yamauchi, M., Fujii, K., Tamura, Y. and Higashino, F. (1993), "Numerical investigation of supersonic flows around a spiked blunt body", *J. Spacecraft Rockets*, **32**(1), 32-42. https://doi.org/10.2514/3.26571.

CC